

# Melting of the $\text{Au}_{20}$ gold cluster : does charge matter?

Mathias Rapacioli,<sup>\*,†</sup> Nathalie Tarrat,<sup>\*,‡</sup> and Fernand Spiegelman <sup>†</sup>

<sup>†</sup>*Laboratoire de Chimie et Physique Quantiques LCPQ/IRSAMC, UMR5626, Université de Toulouse (UPS) and CNRS, 118 Route de Narbonne, F-31062 Toulouse, France.*

<sup>‡</sup>*CEMES, Université de Toulouse, CNRS, 29, rue Jeanne Marvig, 31055 Toulouse, France*

E-mail: mathias.rapacioli@irsamc.ups-tlse.fr; nathalie.tarrat@cemes.fr

## Abstract

We investigate the dependence upon charge of the heat capacities of the magic gold cluster  $\text{Au}_{20}$  obtained from density functional based tight binding theory within parallel tempering molecular dynamics and the multiple histogram method. The melting temperatures, determined from heat capacity curves, are found to be 1102 K for neutral  $\text{Au}_{20}$  and only 866 and 826 K for  $\text{Au}_{20}^+$  and  $\text{Au}_{20}^-$ . The present work proves that a single charge quantitatively affects the thermal properties of the twentymer even for a global property such as melting.

## Introduction

Investigation of the thermodynamical behaviour of small metal clusters has strongly developed since the early investigations by Pauwlov<sup>1</sup> and Buffat and Borel<sup>2</sup> on finite size gold particles, showing that small particles have a lower melting point than bulk materials. After the pioneering nanocalorimetry experiment of Schmidt *et al.*,<sup>3</sup> a couple of experimental techniques<sup>4-6</sup> have made possible the determination of the heat capacity curves of metal clusters

as a function of temperature down to selected sizes as small as typically ten atoms, in particular in the region of the finite size equivalent of the solid-liquid transition. Unlike in the bulk, the transition in finite systems is not abrupt but extends over a finite temperature interval, as formalized by Berry<sup>7</sup> and documented in textbooks.<sup>8,9</sup> Both the melting temperatures and the latent heat have been shown to depend strongly on size.<sup>3</sup> Alkali metal clusters have been specially documented, however caloric curves of other metal particles have also been experimentally obtained. For other types of clusters, the influence of a single impurity<sup>10</sup> or a substrate<sup>11</sup> on the thermal properties has also been documented.

Gold clusters and nanoparticles have been the object of numerous studies, due to their remarkable properties in several application fields such as catalysis, nano-electronics, nano-luminescence or medicine. The structure and static properties of  $\text{Au}_N$  clusters and nanoparticles have been widely investigated, some of the works providing explicit comparison between data from calculated structures (mostly in the DFT framework) and experimental data. However although the early experiment of Buffat and Borel<sup>2</sup> were concerned with gold nanoparticles, no experimental size-selected determination of the caloric curves in the cluster regime range ( $N$  less than 50) has been published so far to our knowledge. A number of theoretical investigations<sup>12-19</sup> usually achieved with many body potentials or thermodynamical models have examined thermodynamically induced structural conversion and melting of large nanoparticles. Simulations of thermal properties were also carried out in the cluster regime size (from one to a few tens). Several works were concerned by simulations of specific thermal behaviours related to 2D-3D transitions in small clusters<sup>20,21</sup> or to thermodynamical aspects of vibrational heating.<sup>22</sup> The caloric curves of gold clusters in the small and medium size range were quite systematically investigated by Soulé du Bas and coworkers.<sup>23,24</sup> In their comparison between  $\text{Au}_{19}$  and  $\text{Au}_{20}$  in particular, they showed that strong differences could be induced by a single missing atom, which is a manifestation of finite size effects where each atom and defect counts. Differential effects were also observed in cage gold clusters.  $\text{Au}_{20}$

is referred to as a magic cluster. The shape of the neutral cluster was found to be a highly symmetric  $T_d$  pyramid that can be viewed as a part of the *fcc* lattice. The shapes of the ionized clusters  $\text{Au}_{20}^+$  and  $\text{Au}_{20}^-$  are also essentially pyramidal, with very small Jahn-Teller deformations from the  $T_d$  symmetry. Those geometries are now well established from theory<sup>25,26</sup> and also from experiment, namely infrared spectroscopy<sup>25</sup> for the neutral species, Trapped Ion Electron Diffraction<sup>26</sup> or Ion mobility<sup>27</sup> techniques for the cation and the anion. The electronic structure of neutral  $\text{Au}_{20}$  can be modeled as a closed shell system with  $1s^2 1p^6 1d^{10} 2s^2$  superorbital configuration for the outer delocalized electrons in the simple spherical Jellium model (eventhough  $5d$  electron bonding and atomic  $6s - 5d$  hybridization can certainly not be neglected). This electronic shell closing together with the symmetric *fcc* packing of  $\text{Au}_{20}$  supports a particular large stability and its magic character in the mass spectra.

In recent works, we have adapted and benchmarked DFTB parameters<sup>28,29</sup> for gold materials from clusters up to bulk.<sup>30</sup> We additionally checked the convergence of the cohesive energies of larger nanoparticles of a few hundreds of atoms to the bulk values, as well as the structural, elastic and energetical properties of bulk itself. As a key advantage, DFTB proved able to yield differential and selective results for charged clusters, namely  $\text{Au}_n^+$  and  $\text{Au}_n^-$  in addition to the neutrals, providing fairly consistent ionization potentials and electron affinities. In a subsequent work, we combined DFTB with a global search algorithm based on the Parallel Tempering Molecular Dynamics (PTMD) scheme<sup>31</sup> completed with periodic quenching to obtain the lowest energy isomers of  $\text{Au}_{20}^{(0,+,-)}$  and  $\text{Au}_{55}^{(0,+,-)}$ . One conclusion of the work for  $\text{Au}_{20}$  was that the isomerization energy gap is related to the specific charge state of the cluster, namely the gap is large for the neutral and much smaller for the anion and the cation. The present work is dedicated to the investigation of the influence of the charge state of the cluster on the heat capacity curves in the temperature region about the solid-liquid transition temperatures in the bulk. Apart of this fundamental aspect, consideration of ions

is also of interest because they can be more easily formed and detected in most experiments. The nature of the phase changes in the interval 100-1700 K and its dependence upon charge is analysed from the caloric curves and the temperature-evolution of the isomer populations.

## Computational details

The potential energy of the neutral, cationic and anionic clusters were determined using the second-order version of DFTB<sup>32-34</sup> (Self-Consistent Charge SCC) and the parameters for gold introduced in our previous publication.<sup>30,35</sup> Note here that the SCC scheme is relevant since it provides a self-consistent account of electrostatics, especially important at the surface of charged metal clusters. The Potential Energy Surface (PES) at various temperatures was explored using classical Molecular Dynamics with Parallel Tempering scheme,<sup>31</sup> as previously implemented<sup>36</sup> in the deMonNano code.<sup>37</sup> This technique strongly enhances the ergodicity in the simulations. For each case, we used a temperature range going from 50 to 2000 K with 60 replica using an exponential distribution of temperatures. The length of each trajectory was 7.5 ns using a timestep of 1.5 fs to integrate the classical equations of motion. Exchanges were attempted using the Metropolis energy criterion every 1.2 ps. We used a Nosé-Hoover chain of thermostats with frequencies of 800 cm<sup>-1</sup> to achieve an exploration in the canonical ensemble. Evaporation did not occur as a crucial problem here, since there is a quite large difference between the solid-liquid and the liquid-gas transition temperatures (respectively 1337 K<sup>38</sup> *vs* 3243 K<sup>39</sup> for the bulk). Nevertheless in order to avoid any problems in the solid-liquid region of the heat capacity, we enclosed the clusters within a large rigid spherical potential centered on the cluster center of mass defined by  $V(r) = a(r - r_0)^8$  with  $a=0.08$  Hartree and  $r_0 = 20 \text{ \AA}$  for  $r > r_0$ . Several approaches exist to determine the heat capacity curve. In the present study, as in the work of Krishnamurty *al.*,<sup>24</sup> we applied the multiple histogram method developed by Labastie and Whetten.<sup>40</sup> This approach reduces the statistical noise and allows to extrapolate heat capacities to temperatures not explicitly simulated.

Finally, the isomer population analysis was done after periodic quenching. For each temperature, 1024 quenches (conjugated gradient optimization), regularly distributed along the trajectory were achieved, allowing to assign the isomer basins (catching areas). Identification of the quenched structures was done combining an energy threshold (difference in energy less than  $10^{-4}$  Hartree) together with an ordered-distances criterion (the interatomic distances based similarity function introduced by Joswig *et al.*<sup>41</sup> with a similarity threshold of 0.95). Note that a number of extra quasi-degenerate isomers, similar however not identical, were obtained with respect to our previous work.<sup>35</sup>

## Results and Discussion

The heat capacity curves are plotted in figure 1. The first noticeable feature is that all three curves are unimodal with a single and well defined peak and that no premelting feature can be inferred from the heat capacities (unlike for instance in Au<sub>17</sub><sup>42</sup>). Since the transition ranges are finite, we will comment here the temperatures  $T_{start}$  at which the transition starts and the temperatures of the peak maxima which will supposedly be considered as the melting temperatures  $T_{melt}$ . One may estimate that the transition starts at the intersection between the low temperature linear raise and the tangent at the inflexion point of the heat capacity. For the neutral cluster,  $T_{start}$  is around 904 K while this non linear raise occurs at lower temperature for the cation and the anion, namely 642 and 551 K. The peak maxima for the neutral, the cation and the anion are located at 1102, 866 and 826 K respectively. Thus the temperature extension range of the transition can be estimated as 396, 448 and 550 K respectively (estimated as the peak bottom width taken as twice the difference between the start and the peak maximum). The present result for the neutral is in qualitative good correspondence with the DFT/LDA work of Krishnamurty *et al.*<sup>24</sup> who also observed a steep raise in the temperature evolution of the root mean square displacement attributed to

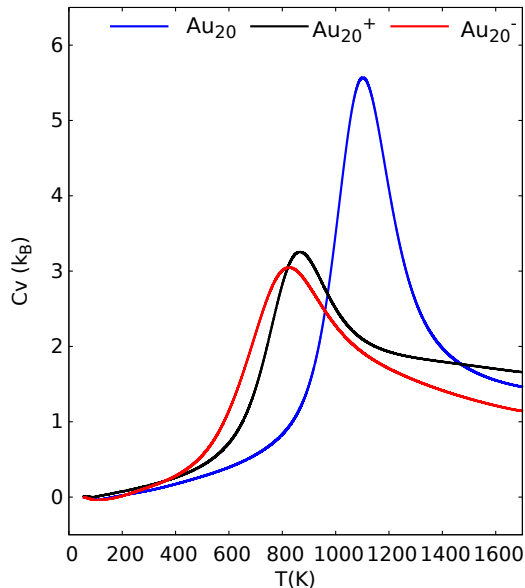


Figure 1: Heat capacity curves for  $\text{Au}_{20}$ ,  $\text{Au}_{20}^+$  and  $\text{Au}_{20}^-$ .

a direct solid-liquid transition for  $\text{Au}_{20}$ . Note that the peak maximum in the present work is shifted to significantly higher temperatures, likely due to the larger isomerization energies in DFTB *vs* LDA. Let us mention that the DFT isomerization energies may significantly depend on the functional used. Actually, the present DFTB first gap to isomerization (0.64 eV) is in much better correspondence with the DFT/TPSS gap of Letchken *et al.*<sup>26</sup> (0.75 eV) than with the DFT/LDA results (0.44 eV). The width of the phase change interval ( $\sim 400$  K) in the present DFTB simulation is nevertheless consistent with the heat capacity data of Krishnamurty *et al.*<sup>24</sup>

The original outcome of the present work concerns ions and shows that there is a significant reduction of the melting temperature for charged clusters with identical size, and even a perceivable difference can be made between the cation and the anion. The DFTB isomers structural excitation energies are reported in fig 2. Note that the quenching procedure used here (achieving quenches from all the MDPT trajectories at all the samples temperatures) generated extra isomers in addition to those of our previous work among the 15 lowest ones for each charge state. As mentioned above, the lowest energy isomer of all three species is a pyramidal-like *fcc* structure. One may also mention that quasi-degenerate isomers with

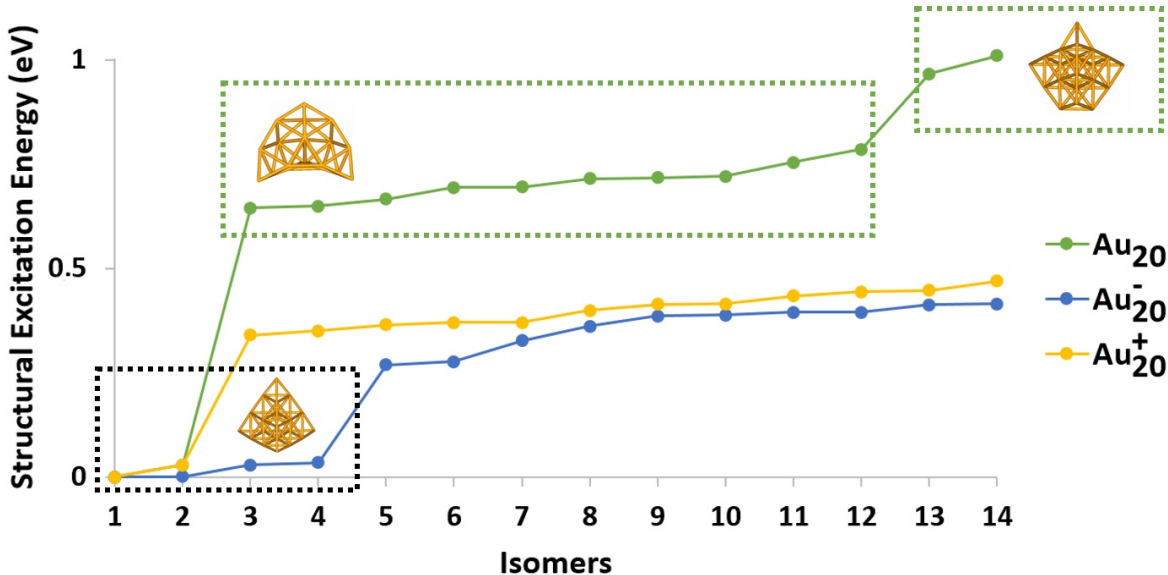


Figure 2: Structural excitation energies of the 14th lowest energy isomers of Au<sub>20</sub> (green), Au<sub>20</sub><sup>+</sup> (yellow) and Au<sub>20</sub><sup>-</sup> (blue). Isomers belonging to the same meta-basin are framed using boxes (see supporting information).

this lowest energy structure are obtained consisting of very small distortions. In the ions, these correspond to various Jahn-Teller distortions, generating several, almost isoenergetic isomers. The above deformations only affect the T=0 K limit of the heat capacities, however they do not create any visible associated feature on the heat capacity curves. Note that the T=0 K limit cannot be properly described in the present work due to the neglect of quantum effects. Let us however note that several groups of quasi-degenerate isomers with very neighboring topologies can be found below 1 eV. For instance, isomers 3-12 of the neutral are distinct but they only differ by one or two bond or a small distortion (see Supplementary Information figure 2). Such sets of isomers may be thought of as defining meta-basins of the PES. The main differences between the neutral, the cations and the anions however concern the first non-pyramidal isomers. In Au<sub>20</sub>, the set of isomers 3-12 lie in the range 0.64-0.79 eV above the lowest one and the isomerization energy of the next one (13) is 0.97 eV, not considering the barriers. In the cation, the isomerisation energy to isomer 4 is 0.34 eV. In the anion, the isomerisation energy to isomer 5 is 0.27 eV. Both are significantly smaller

than the corresponding gap for the neutral. A continuous progression above the first gap is observed. Again this decrease of the structural excitation energies above the pyramid meta-basin for ions with respect to the neutral are in reasonable correspondence with the DFT/TPSS values of Lechtken.<sup>26</sup>

Insight in the atomistic aspect of melting can be gained in the analysis of the isomer basin populations. In the neutral case, it appears that the decrease of the population of the pyramidal isomer starts around 800 K. The decrease is quite regular, not showing any steps, and the depletion is fully achieved around 1300 K. Only a single meta-basin (isomers in the range 0.64-0.76 eV, essentially isomer 5) contributes with a visible population (however minor < 10 percent at its maximum) within the melting temperature range, namely 700-1200K and then disappears at higher temperature. The main observation for  $T \geq 900$  K, is a growing population consisting of a collection of many different higher energy isomers (labeled "others" in fig 3), revealing strong geometrical fluctuations, so that the cluster can be considered as melted. The minor contribution of some meta-basin structures 3-12 thus appears more as a prelude of a direct and continuous solid-to-liquid transition than as a solid-to-solid transition. Almost all the lowest isomers are essentially generated by the migration of a corner atom (possibly two ) to a face of the pyramidal cluster, inducing possible distortions. Those results are qualitatively consistent with the conclusion of the DFT/LDA simulation of Krishnamurty *et al.*,<sup>24</sup> despite of the quantitative differences in the melting temperatures between the two calculations.

The melting mechanisms corresponding to ionized species are similar. For the cation case, depletion of the pyramidal lowest energy structure starts as soon as 450-500K while populations of isomers 3,4,7 and above somewhat increase up to a maximum. At higher temperature, these population decrease, while isomers labeled "others" become predominant as in the neutral case. In the anion none of the low-energy isomers is ever significantly populated. Thus as for the neutral clusters, melting appears as a direct and continuous solid-



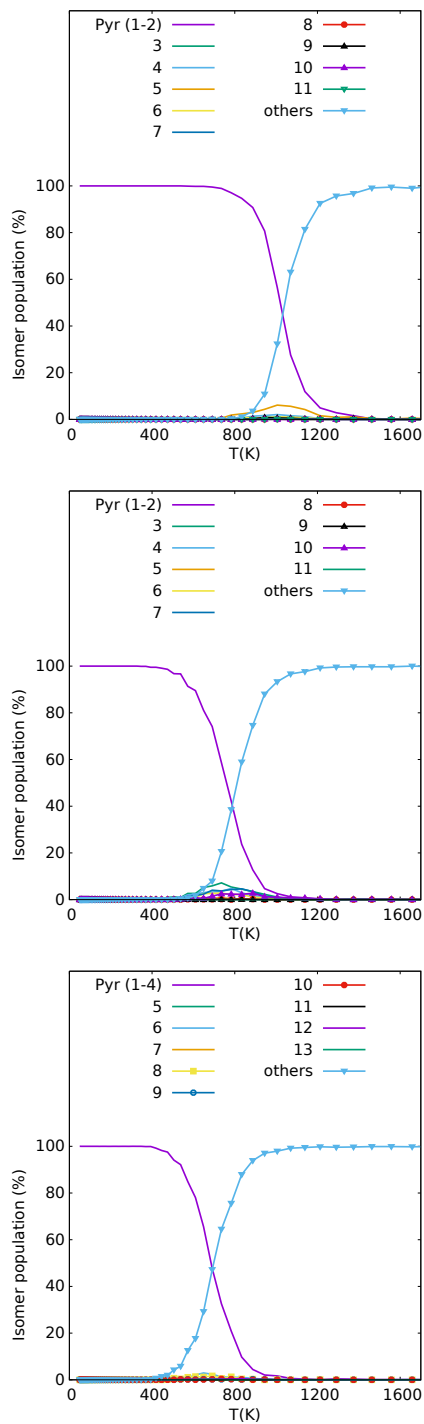


Figure 3: Temperature evolution of the isomer population as a function of Temperature for Au<sub>20</sub> (top), Au<sub>20</sub><sup>+</sup> (center) and Au<sub>20</sub><sup>-</sup> (bottom).

liquid transition, however shifted to lower temperatures, due to the lowest energy needed for the departure from the pyramid basins. In no cases any onset of a solid-to-solid type premelting feature can be significantly observed.

## Conclusion

Using the DFTB approach and canonical PTMD exploration scheme, we have achieved a comparative analysis of the heat capacity curves of  $\text{Au}_{20}$ ,  $\text{Au}_{20}^+$  and  $\text{Au}_{20}^-$  as a function of temperature. The melting temperatures are estimated at 1102 K, 866 K and 826 K respectively. The present work shows that the change in the potential energy landscape induced by the cluster charge yields a significant variation in the energetical distribution of the low energy isomers and results in a quantitatively different solid-to-liquid transition temperature. Nevertheless, in all cases the transition is found to correspond to direct melting. This extends the findings of Krishnamurty *et al.*<sup>24</sup> addressing thermodynamical finite size effects for gold. Although this difference will evidently vanish for large nanoparticles, the present work evidences charge effects in clusters, namely the influence of an extra charge, even unity. This was already known for electronic stability for instance but is evidenced here also for a thermal global quantity such as the heat capacity in this medium size range, which still is shown to be strongly determined not only by the atom count, but also by the electron count.

## Acknowledgements

This work was granted access to the HPC resources of CALMIP (Grants p1303 and p0059) and from IDRIS (Grant i2015087375). It was supported by a CNRS-Inphyniti Grant (ATHENA project), the CNRS-GDR EMIE and the NEXT grants ANR-10-LABX-0037 in the framework of the *Programme des Investissements d'Avenir* (CIM3 and EXTAS projects).

## Supporting Information Available

The following files are available free of charge. Structures of isomers 3 to 14 of Au<sub>20</sub>.

## References

- (1) Pawlow, P. *Z. Phys. Chem* **1909**, *65*, 1–35.
- (2) Buffat, P.; Borel, J.-P. *Phys. Rev. A* **1976**, *13*, 2287–2298.
- (3) Schmidt, M.; Kusche, R.; von Issendorff, B.; Haberland, H. *Nature* **393**, 238–240.
- (4) Breaux, G. A.; Benirschke, R. C.; Sugai, T.; Kinnear, B. S.; Jarrold, M. F. *Phys. Rev. Lett.* **2003**, *91*, 215508.
- (5) Chirof, F.; Feiden, P.; Zamith, S.; Labastie, P.; L’Hermite, J.-M. *The Journal of Chemical Physics* **2008**, *129*, 164514.
- (6) Boulon, J.; Braud, I.; Zamith, S.; Labastie, P.; Jean-Marc L’Hermite, *The Journal of Chemical Physics* **2014**, *140*, 164305.
- (7) Berry, R. S. *Sci. Am.* **1990**, *263*, 50–56.
- (8) Wales, D. *Energy Landscapes: Applications to Clusters, Biomolecules and Glasses*; Cambridge Molecular Science; Cambridge University Press, 2004.
- (9) Labastie, P.; Calvo, F. *Nanomaterials and Nanochemistry*; Springer, 2007; pp 55–87.
- (10) Douady, J.; Calvo, F.; Spiegelman, F., *Eur. Phys. J. D* **2009**, *52*, 47–50.
- (11) Oliveira, L. F. L.; Cuny, J.; Moriniere, M.; Dontot, L.; Simon, A.; Spiegelman, F.; Rapacioli, M. *Phys. Chem. Chem. Phys.* **2015**, *17*, 17079–17089.
- (12) Castro, T.; Reifengerger, R.; Choi, E.; Andres, R. P. *Phys. Rev. B* **1990**, *42*, 8548–8556.

- (13) Lewis, L. J.; Jensen, P.; Barrat, J.-L. *Phys. Rev. B* **1997**, *56*, 2248–2257.
- (14) Cleveland, C. L.; Luedtke, W. D.; Landman, U. *Phys. Rev. Lett.* **1998**, *81*, 2036–2039.
- (15) Cleveland, C. L.; Luedtke, W. D.; Landman, U. *Phys. Rev. B* **1999**, *60*, 5065–5077.
- (16) Wang, Y.; Teitel, S.; Dellago, C. *Chemical Physics Letters* **2004**, *394*, 257 – 261.
- (17) Ruiz Gómez, J. C.; Rincón, L. *Rev. Mex. Phys.* **2007**, *53*, 208,211.
- (18) Golovenko, Z. V.; Ya., G. Y.; L., G. S.; V., R. L. *The Physics of metals and Metallography* **2013**, *114*, 1038–1944.
- (19) Gafner, Y. Y.; Gafner, S. L.; Zamulin, I. S.; Redel, L. V.; Baidyshev, V. S. *The Physics of Metals and Metallography* **2015**, *116*, 568–575.
- (20) Koskinen, P.; Häkkinen, H.; Huber, B.; von Issendorff, B.; Moseler, M. *Phys. Rev. Lett.* **2007**, *98*, 015701.
- (21) Li, J.; Lin, D.; Chen, C.; Li, Q.; L, L.; Sun, R.; Juang, S.; Wang, Z. *J. Appl. Phys.* **2015**, *117*, 085303–085310.
- (22) K, V.; M, S. *Journal of Material Sciences and Engineering* **2017**, *6*, 1–15.
- (23) Soulé de Bas, B.; Ford, M. J.; Cortie, M. B. *Journal of Physics: Condensed Matter* **2006**, *18*, 55–74.
- (24) Krishnamurty, K.; Shafai, G. S.; Kanhere, D. G.; Soulé de Bas, B.; Ford, M. J. *J. Phys. Chem. A* **2007**, *111*, 10769 – 10775.
- (25) Gruene, P.; Rayner, D. M.; Redlich, B.; van der Meer, A. F. G.; Lyon, J. T.; Meijer, G.; Fielicke, A. *Science* **2008**, *321*, 674–676.
- (26) Lechtken, A.; Neiss, C.; Stairs, J.; Schooss, D. *The Journal of Chemical Physics* **2008**, *129*, 154304.

- (27) Furche, F.; Ahlrichs, R.; Weis, P.; Jacob, C.; Gilb, S.; Bierweiler, T.; Kappes, M. M. *J. Chem. Phys.* **2002**, *117*, 6982–6990.
- (28) Koskinen, P.; Häkkinen, H.; Seifert, G.; Sanna, S.; Frauenheim, T.; Moseler, M. *New J. Phys.* **2006**, *8*, 9.
- (29) Fihey, A.; Hettich, C.; Touzeau, J.; Maurel, F.; Perrier, A.; Köhler, C.; Aradi, B.; Frauenheim, T. *J. Comput. Chem.* **2015**, *36*, 2075–2087.
- (30) Oliveira, L. F. L.; Tarrat, N.; Cuny, J.; Morillo, J.; Lemoine, D.; Spiegelman, F.; Rapacioli, M. *The Journal of Physical Chemistry A* **2016**, *120*, 8469–8483.
- (31) Sugita, Y.; Okamoto, Y. *Chem. Phys. Lett.* **1999**, *314*, 141–151.
- (32) Porezag, D.; Frauenheim, T.; Köhler, T.; Seifert, G.; Kaschner, R. *Phys. Rev. B* **1995**, *51*, 12947–12957.
- (33) Seifert, G.; Porezag, D.; Frauenheim, T. *Int. J. Quantum Chem.* **1996**, *58*, 185–192.
- (34) Elstner, M.; Porezag, D.; Jungnickel, G.; Elsner, J.; Haugk, M.; Frauenheim, T.; Suhai, S.; Seifert, G. *Phys. Rev. B* **1998**, *58*, 7260–7268.
- (35) Tarrat, N.; Rapacioli, M.; Cuny, J.; Morillo, J.; Heully, J.-L.; Spiegelman, F. *Computational and Theoretical Chemistry* **2017**, *1107*, 102–114.
- (36) Oliveira, A. F.; Philippsen, P.; Heine, T. *J. Chem. Theory Comput.* **2015**, *11*, 5209–5218.
- (37) Heine, T.; Rapacioli, M.; Patchkovskii, S.; Cuny, J.; Frenzel, J.; Koster, A.; Calaminici, P.; Duarte, H. A.; Escalante, S.; Flores-Moreno, R.; Goursot, A.; Reveles, J.; Salahub, D.; Vela, A. deMonNano, <http://demon-nano.ups-tlse.fr/>, 1st Sept 2016.
- (38) Kaye, G.; Laby, T. *Tables of physical and chemical constants*, Longman, London, UK, 15th edition,; 1993.

- (39) Zhang, Y.; Evans, J. R. G.; Yang, S. *Journal of Chemical & Engineering Data* **2011**, *56*, 328–337.
- (40) Labastie, P.; Whetten, R. L. *Phys. Rev. Lett.* **1990**, *65*, 1567–1570.
- (41) Joswig, J.-O.; Lorenz, T. *Detecting and Quantifying Geometric Features in Large Series of Cluster Structures*; 2016; Vol. 230.
- (42) Chandrachud, P.; Joshi, K.; Krishnamurty, S.; Kanhere, D. G. *Pramana* **2009**, *72*, 845–855.

# Graphical TOC Entry

